This article has been accepted for publication in a future issue of this journal, but has not been fully edited. Content may change prior to final publication. Citation information: DOI 10.1109/TSP.2017.2679693, IEEE Transactions on Signal Processing

Joint Threshold Adjustment and Power Allocation for Cognitive Target Tracking in Asynchronous Radar Network

Junkun Yan, *Member, IEEE*, Hongwei Liu, *Member, IEEE*, Wenqiang Pu, Hongliang Liu, Zheng Liu, Zheng Bao, *Life senior Member, IEEE*

***Abstract*—In this paper, a *joint threshold adjustment and power allocation* (JTAPA) algorithm is developed for target tracking in *asynchronous radar network* (ARN). The basis of the JTAPA strategy is to feed back the target track information from the fusion center to local radar sites to enhance both the target detection capability and the resource utilization efficiency of the ARN. For the detector, we develop a *threshold adjustment* (TA) algorithm for better detection performance, based on the predicted target location information fed back from the fusion center. For the transmitter, we build an *asynchronous power allocation* (APA) model based on the perceptual information, and use optimization technique to control the limited power resource for the next period of time. The goal of the APA scheme is to achieve better target tracking accuracy with a given power budget. The Bayesian Cramér-Rao lower bound is derived, normalized, and subsequently utilized, as the optimization criterion for the APA strategy. The resulting nonconvex optimization problem is solved through relaxation incorporating the spectral projected gradient technique. Simulation results demonstrate that the integration of the TA and APA processes can evidently improve the tracking performance.**

***Index Terms*—Asynchronous Radar network, Cognitive, Resource allocation, Target detection, Target tracking**

I. Introduction

A. Background and Motivation

Recently, many surveillance systems have been relying on multiple radars which can work together in a coordinated way. Radar network has already been shown to have a number of potential advantages over monostatic radar [1]-[8], and thus it could be used to detect and track targets for defense purposes.

In traditional multistatic tracking system, the information flows only one way: from local radar sites to the *fusion center* (FC). In such a framework, prior information obtained from the previous recursion cycle in target tracking is not fed back from the FC to each site, e.g. the predicted target state and the target *radar cross section* (RCS) information [4]. Thus, the prior information neither accounts for the properties of the detector, nor cares for the resource utilization efficiency objective. If the prior information can be used in a cognitive manner [9],[10] both at the detector [11] and the transmitter [5], the detection performance [6] , as well as the resource utilization efficiency [7] could be evidently improved. Herein, the expression 'cognitive' is meant to guide the detectors where to look for a target, and adjust the transmitters to better perceive the target according to the prior information provided by the FC [12].

Previously, extensive efforts have been made to analyze the cognitive target detection and tracking strategy in radar network, and the existing works can be classified into two categories. The first type is to feed back the track information for an improved detection performance [11],[13],[14], and we refer it to the *cognitive detection* (CD) technique. Reference [13] considers the problem of detection threshold optimization so that a feedback from the tracker to the detector is formed to maximize the target tracking performance. Rather than optimizing the threshold, a Bayesian detector is proposed in [11], and the feedback information is the predicted distribution of the target location. Later, reference [6] extends this work to the synchronous netted radar platform. The perceptual information is then utilized to guide the detectors of multiple radars where to look for a target while keeping the constant *false alarm rate* (FAR) property. As an alternative, reference [15] and [16] analyze a decentralized and collaborative detection scheme, in which each node exchanges target information with its neighboring nodes without any fusion center. The latter type of the cognitive processing works is to adaptively allocate the limited resource of the radar network based on the feedback information, with the aim of achieving better target tracking accuracy under some specified resource constraints [7],[17],[18]. In this paper, we refer this to the *cognitive transmitting* (CT) process.

The aforementioned works show that both the CD and CT processes can enhance the target tracking performance with the utilization of the prior information. However, there still exist many aspects need to be further improved: (a) Most of the existing works adopt synchronous measurement model, which is not appropriate for the practical extension of the researches. In real application, the target data reported by multiple radars are usually asynchronous due to different sampling rates; (b) Most of the existing works conduct the CD and CT processes separately. For CD, the transmit parameters are predefined, the prior information is fed back to facilitate target detection only [6],[11]; As for CT, an ideal detection precondition is assumed: (a) the *probability of detection* (PD) is one; (b) the FAR is zero. In this scenario, the notion of CD is unnecessary, and the prior

This work is partially supported by the National Natural Science Foundation of China (61601340), the National Science Fund for Distinguished Yong Scholars (61525105), the Postdoctoral Science Foundation of China (2015M580817, 2016T90890), the Postdoctoral Scientific Research Project Fund of Shaanxi, and the Fundamental Research Funds for the Central Universities (JB160227, XJS15051).

The authors are with the National Laboratory of Radar Signal Processing, and Collaborative Innovation Center of Information Sensing and Understanding at Xidian University, Xi'an, China.

This article has been accepted for publication in a future issue of this journal, but has not been fully edited. Content may change prior to final publication. Citation information: DOI 10.1109/TSP.2017.2679693, IEEE Transactions on Signal Processing

information is only used for resource allocation [7],[17].

In view of the aforementioned problems, we integrate the advantages of the CD and CT processes into a coherent framework, and develop a *joint threshold adjustment and power allocation* (JTAPA) algorithm for target tracking in *asynchronous radar network* (ARN). In this model, the closed-loop JTAPA algorithm constitutes a form of feedback from the FC to the detector, as well as the transmitter of each site. For the detector, the feedback information is the predicted distribution of the target location, and then the location dependent threshold is depressed near where a target is expected to be and elevated where it is unexpected. For the transmitter, we build an *asynchronous power allocation* (APA) model, and adjust the transmit power of each radar according to the feedback information. Specifically, as the *Bayesian Cramér-Rao lower bound* (BCRLB) is one of the most important information that can be used to quantify the target tracking performance [19], we use optimization technique to manage the limited power resource of the ARN for the purpose of minimizing a cost function based on the BCRLB. In this scenario, the feedback information for the transmitter is actually the predicted BCRLB.

B. Main Contributions

The major contributions of this paper are as follows:

(1) *A closed-loop threshold adjustment* (TA) *method is developed based on a predefined track confirmation rule and the feedback from the FC.* In early works [20], the value of FAR is empirically set as a very small value, such as 10^{-6}, in view of the computational capacity of the FC in handling maximum number of false alarms from multiple local radars. With the recent development in electronic component technology, FC can deal with more data simultaneously. Therefore, it might be an intuitive idea to decrease the threshold of each radar, in hope that the target detection probability could be improved. In order to enhance PD, the proposed TA algorithm will incorporate two kinds of technical means: (a) Slightly decrease the detection threshold, while constraining the *false track rate* (FTR) to be a required value [21]. In such a case, the number of the false alarms is also constrained [20]; (b) Set a location dependent Bayesian threshold according to the feedback information as [6]. Due to this property, the PD of each radar must averagely be calculated over the tracking gate, with a given averaged FTR. Then, the closed-loop TA algorithm might be seen as an updated version of the works developed in [6] and [21].

(2) *An APA algorithm for target tracking in ARN is proposed based on the feedback from the FC.* In ARN, the sampling intervals of distinct radars are different, and thus we map the sampling time of individual radar into a global time axis sequentially, and build the global target tracking model. Unlike the synchronous cases [7],[17], in which the power allocation strategy is carried out for all the radars at each time index, the APA strategy allocate the limited system power resource for the next period of time (Hereafter, we refer it to the allocation period). For each allocation period, the BCRLB is recursively derived, normalized, and subsequently utilized, as the optimization criterion for the power allocation strategy. The optimization framework results in a nonconvex, nonlinear, optimization problem. To solve this problem, we first choose an appropriate relaxation of the objective function, and then use the optimal solution as a start point to find a constrained stationary point for the original nonconvex problem, through the *spectral projected gradient* (SPG) algorithm [22].

(3) *Integrating the advantages of the CD and CT techniques into a coherent framework, we develop a closed-loop JTAPA algorithm for cognitive target tracking in ARN.* On one hand, the TA technique, which can be viewed as a CD scheme, consists of a feedback from the FC to the detector of each node. On the other hand, the APA strategy, which is actually a CT scheme, consists of another feedback from the FC to the transmitter of each node. Therefore, the JTAPA algorithm developed in this paper is composed of two feedbacks. Specifically, the feedbacks are as follows: (a) At each global time index, the detection threshold is properly set in a Bayesian form based on the predicted target location, and is slightly decreased according to a predefined track confirmation rule; (b) At each allocation period, the APA model is built based on the predicted BCRLB, and the illumination parameters for the next period of time can be obtained by solving the resulting optimization problem. Within this closed-loop cognitive framework, we collect the measurements from different radars that exceed their own detection threshold, and use the *joint detection and tracking processing* (JDTP) algorithm developed in [6] to achieve the target state at each global time index.

The rest of the paper is structured as follows: Section II formulates the system model. In Section III, the TA strategy is developed for the detector of each node. Then, the APA scheme is built in Section IV. The basis of the APA scheme is introduced in Section IV-A. Section IV-B derives the mathematical optimization model of the APA strategy. The resulting nonconvex optimization problem is solved by relaxation method incorporating the SPG technique in Section IV-C. In Section IV-D, the JDTP algorithm [6] is adopted to achieve the state estimation, and then the general steps of the closed-loop JTAPA algorithm are given. Several numerical results are provided in Section V to verify the effectiveness of the proposed JTAPA technique. Finally, the conclusion of the paper is made in Section VI.

II. System Model

Without loss of generality, we consider an ARN with N spatially diverse monostatic radars. These radars are labeled $1,2,...,N\left(N \geq 2\right)$ with the location of the j th radar denoted by $\left(x_j, y_j\right)$. We assume that: (a) Each radar transmits a signal with different carrier frequency $f_{c,j}$; (b) The radar station j is equipped with only a matched filter that correlates to its own transmitted signal. Thus, any radar station can receive its own signal, and the target echoes from the other signals generate near-zero outputs at the matched filter because it does not correlate with any of them. In this case, each radar operates in a monostatic way, and sends its thresholded data to the FC.

A. Target Model

Target motion is prescribed by a constant velocity model

This article has been accepted for publication in a future issue of this journal, but has not been fully edited. Content may change prior to final publication. Citation information: DOI 10.1109/TSP.2017.2679693, IEEE Transactions on Signal Processing

$$\dot{\mathbf{x}}^c(t)=\mathbf{A}\mathbf{x}^c(t)+\mathbf{u}(t), \tag{1}$$

where $\mathbf{A}$ is the system matrix, $\mathbf{x}^c(t)$ is the continuous time system state at time t and $\mathbf{u}(t)$ is a zero mean white Gaussian process noise with covariance [23],[24]

$$\mathbb{E}\left[\mathbf{u}(t)\mathbf{u}^T(\tau)\right]=\mathbf{q}(t)\delta(t-\tau) \tag{2}$$

where $\mathbb{E}$ is the mathematical expectation operator, and $\mathbf{q}(t)$ is the power spectral density of the process noise [24] at time t.

In practice, radars generally have different tasks, and thus the sampling interval of the i th radar T_i might be different from that of others. To update the target state, we map the sampling time of individual radar into a global time axis k_{G} sequentially. In this scenario, the tracking interval at the FC is non-uniformly spaced, see Fig. 1 for detail. To facilitate derivation, we define a variable $n_{k_{\mathrm{G}}}$ to denote the number of the measurements at time index k_{G}, and use the vector $\mathbf{i}_{k_{\mathrm{G}}}$ to record the origination of the measurements. Thus, we know that the j th measurement at time index k_{G} is from radar $\mathbf{i}_{k_{\mathrm{G}}}(j)$, $j=1,\ldots,n_{k_{\mathrm{G}}}$.

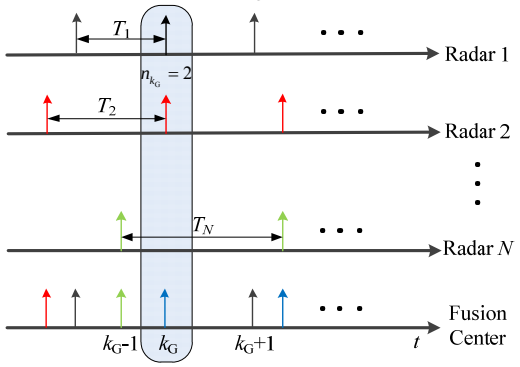

Fig. 1 Sketch map of the asynchronous sampling model. At each global time index k_{G}, the observations consist of the measurement from radar $\mathbf{i}_{k_{\mathrm{G}}}(j)$, $j=1,\ldots,n_{k_{\mathrm{G}}}$

In this model, the target state evolves between two indices on the global time axis, and the discrete dynamic model is [23]

$$\mathbf{x}_{k_{\mathrm{G}}}=\mathbf{F}_{\mathbf{x}}(k_{\mathrm{G}},k_{\mathrm{G}}-1)\mathbf{x}_{k_{\mathrm{G}}-1}+\mathbf{u}(k_{\mathrm{G}},k_{\mathrm{G}}-1) \tag{3}$$

where the target state is given by $\mathbf{x}_{k_{\mathrm{G}}}=\left[x_{\mathrm{T}k_{\mathrm{G}}},\dot{x}_{\mathrm{T}k_{\mathrm{G}}},y_{\mathrm{T}k_{\mathrm{G}}},\dot{y}_{\mathrm{T}k_{\mathrm{G}}}\right]^T$, with a dimension of $n_{\mathbf{x}}=4$. $\left(x_{\mathrm{T}k_{\mathrm{G}}},y_{\mathrm{T}k_{\mathrm{G}}}\right)$ and $\left(\dot{x}_{\mathrm{T}k_{\mathrm{G}}},\dot{y}_{\mathrm{T}k_{\mathrm{G}}}\right)$ denote the position and velocity of the target, respectively. $\mathbf{F}_{\mathbf{x}}(k_{\mathrm{G}},k_{\mathrm{G}}-1)$ is the discrete state transition matrix [24]

$$\begin{cases}\mathbf{F}_{\mathbf{x}}(k_{\mathrm{G}},k_{\mathrm{G}}-1)=\boldsymbol{\varphi}\left(t_{k_{\mathrm{G}}},t_{k_{\mathrm{G}}-1}\right)=\exp\left[\mathbf{A}\left(t_{k_{\mathrm{G}}}-t_{k_{\mathrm{G}}-1}\right)\right]\\ \mathbf{u}(k_{\mathrm{G}},k_{\mathrm{G}}-1)=\int_{t_{k_{\mathrm{G}}-1}}^{t_{k_{\mathrm{G}}}}\boldsymbol{\varphi}\left(t_{k_{\mathrm{G}}},\tau\right)\mathbf{u}(\tau)d\tau\end{cases} \tag{4}$$

The term $\mathbf{u}(k_{\mathrm{G}},k_{\mathrm{G}}-1)$ denotes the discrete process noise, and is assumed to be zero-mean, Gaussian with a covariance [24]

$$\mathbf{Q}(k_{\mathrm{G}},k_{\mathrm{G}}-1)=\int_{t_{k_{\mathrm{G}}-1}}^{t_{k_{\mathrm{G}}}}\boldsymbol{\varphi}\left(t_{k_{\mathrm{G}}},\tau\right)\mathbf{q}(\tau)\boldsymbol{\varphi}^T\left(t_{k_{\mathrm{G}}},\tau\right)d\tau \tag{5}$$

The transition model of the target RCS is assumed to be a first order Markovian process [7], [17] and is described by the following equation:

$$\boldsymbol{\eta}_{k_{\mathrm{G}}}=\boldsymbol{\eta}_{k_{\mathrm{G}}-1}+\boldsymbol{\mu}_{k_{\mathrm{G}}-1} \tag{6}$$

The noise $\boldsymbol{\mu}_{k_{\mathrm{G}}-1}$ is white Gaussian with a known covariance $\mathbf{Q}_{\boldsymbol{\eta},k_{\mathrm{G}}-1}$ (estimated from its historical data in a maximum likelihood sense [25]). The term $\boldsymbol{\eta}_{k_{\mathrm{G}}}=\left[\boldsymbol{\eta}_{1,k_{\mathrm{G}}}^T,\boldsymbol{\eta}_{2,k_{\mathrm{G}}}^T,\cdots\boldsymbol{\eta}_{N,k_{\mathrm{G}}}^T\right]^T$ represents the channel state vector ($\boldsymbol{\eta}_{i,k_{\mathrm{G}}}=\left[\eta_{i,k_{\mathrm{G}}}^R,\eta_{i,k_{\mathrm{G}}}^I\right]^T$), where $\eta_{i,k_{\mathrm{G}}}^R$ and $\eta_{i,k_{\mathrm{G}}}^I$ are the real and imaginary parts of the target RCS with respect to radar i. Now, we form an extended state vector for the target by concatenating the target state vector and the channel state vector into a single vector of dimension $n_{\mathbf{x}}+2N$, which can be defined as $\boldsymbol{\xi}_{k_{\mathrm{G}}}=\left(\mathbf{x}_{k_{\mathrm{G}}}^T,\boldsymbol{\eta}_{k_{\mathrm{G}}}^T\right)^T$. The state transition equation for $\boldsymbol{\xi}_{k_{\mathrm{G}}}$ is then

$$\boldsymbol{\xi}_{k_{\mathrm{G}}}=\mathbf{F}(k_{\mathrm{G}},k_{\mathrm{G}}-1)\boldsymbol{\xi}_{k_{\mathrm{G}}-1}+\boldsymbol{\gamma}(k_{\mathrm{G}},k_{\mathrm{G}}-1) \tag{7}$$

where $\mathbf{F}(k_{\mathrm{G}},k_{\mathrm{G}}-1)$ is the overall transition matrix

$$\mathbf{F}(k_{\mathrm{G}},k_{\mathrm{G}}-1)=\begin{bmatrix}\mathbf{F}_{\mathbf{x}}(k_{\mathrm{G}},k_{\mathrm{G}}-1) & \mathbf{0}_{n_{\mathbf{x}}\times 2N}\\ \mathbf{0}_{2N\times n_{\mathbf{x}}} & \mathbf{I}_{2N}\end{bmatrix} \tag{8}$$

The term $\boldsymbol{\gamma}(k_{\mathrm{G}},k_{\mathrm{G}}-1)$ is the corresponding Gaussian process noise with zero mean and covariance

$$\mathbf{Q}_{\xi}(k_{\mathrm{G}},k_{\mathrm{G}}-1)=\mathrm{blkdiag}\left\{\mathbf{Q}(k_{\mathrm{G}},k_{\mathrm{G}}-1),\mathbf{Q}_{\boldsymbol{\eta},k_{\mathrm{G}}-1}\right\} \tag{9}$$

In (9), the operator $\mathrm{blkdiag}\{\bullet\}$ denotes the block diagonal matrix. Hereafter, when we say state vector, we refer to the augmented state vector $\boldsymbol{\xi}_{k_{\mathrm{G}}}$.

B. Measurement Model at each Node

For target tracking in clutter, we may receive multiple measurements at each time index k_{G}. Let $m_{j,k_{\mathrm{G}}}$ denotes the number of the measurements received by radar j ($j\in\mathbf{i}_{k_{\mathrm{G}}}$) at time index k_{G}, and these measurements can be denoted as

$$\mathbf{Z}_{j,k_{\mathrm{G}}}=\left\{\mathbf{z}_{j,k_{\mathrm{G}}}^l\right\}_{l=1}^{m_{j,k_{\mathrm{G}}}},\quad j\in\mathbf{i}_{k_{\mathrm{G}}} \tag{10}$$

Each measurement $\mathbf{z}_{j,k_{\mathrm{G}}}^l$ has the general form [6]

$$\mathbf{z}_{j,k_{\mathrm{G}}}^l=\begin{cases}\mathbf{h}_j\left(\boldsymbol{\xi}_{k_{\mathrm{G}}}\right)+\mathbf{w}_{j,k_{\mathrm{G}}} & \text{if target generated}\\ \boldsymbol{\upsilon}_{j,k_{\mathrm{G}}} & \text{if false alarm}\end{cases}, \tag{11}$$

where $\mathbf{h}_j\left(\boldsymbol{\xi}_{k_{\mathrm{G}}}\right)$ is the measurement function

$$\mathbf{h}_j(\bullet)=\left[h_{j,R}(\bullet),h_{j,\theta}(\bullet),h_{j,f}(\bullet),h_{j,\eta}^R(\bullet),h_{j,\eta}^I(\bullet)\right]^T. \tag{12}$$

with

$$\begin{cases}R_{j,k_{\mathrm{G}}}=h_{j,R}\left(\boldsymbol{\xi}_{k_{\mathrm{G}}}\right)=\sqrt{\left(x_{\mathrm{T}k_{\mathrm{G}}}-x_j\right)^2+\left(y_{\mathrm{T}k_{\mathrm{G}}}-y_j\right)^2}\\ \theta_{j,k_{\mathrm{G}}}=h_{j,\theta}\left(\boldsymbol{\xi}_{k_{\mathrm{G}}}\right)=\arctan\left[\left(y_{\mathrm{T}k_{\mathrm{G}}}-y_j\right)/\left(x_{\mathrm{T}k_{\mathrm{G}}}-x_j\right)\right]\\ f_{j,k_{\mathrm{G}}}=h_{j,f}\left(\boldsymbol{\xi}_{k_{\mathrm{G}}}\right)=-\dfrac{2}{\lambda_j}\left(\dot{x}_{\mathrm{T}k_{\mathrm{G}}},\dot{y}_{\mathrm{T}k_{\mathrm{G}}}\right)\begin{pmatrix}x_{\mathrm{T}k_{\mathrm{G}}}-x_j\\ y_{\mathrm{T}k_{\mathrm{G}}}-y_j\end{pmatrix}\Big/R_{j,k_{\mathrm{G}}}\\ \eta_{j,k_{\mathrm{G}}}^R=h_{j,\eta}^R\left(\boldsymbol{\xi}_{k_{\mathrm{G}}}\right)=\left(\mathbf{e}_{n_{\mathbf{x}}+2j-1}^{n_{\mathbf{x}}+2N}\right)^T\boldsymbol{\xi}_{k_{\mathrm{G}}}\\ \eta_{j,k_{\mathrm{G}}}^I=h_{j,\eta}^I\left(\boldsymbol{\xi}_{k_{\mathrm{G}}}\right)=\left(\mathbf{e}_{n_{\mathbf{x}}+2j}^{n_{\mathbf{x}}+2N}\right)^T\boldsymbol{\xi}_{k_{\mathrm{G}}}\end{cases}. \tag{13}$$

corresponding to different measurement components [4]. Hence, we have $n_{\mathbf{z}}=5$. In practice, these measurements can be extracted from the radar data using maximum likelihood methods [20]. In (13), λ_i denotes the carrier wavelength, $\mathbf{e}_i^j$ is

This article has been accepted for publication in a future issue of this journal, but has not been fully edited. Content may change prior to final publication. Citation information: DOI 10.1109/TSP.2017.2679693, IEEE Transactions on Signal Processing

a zero vector of length j with the i th element to be one.

We assume that the measurement error $\mathbf{w}_{j,k_G}$ is zero-mean, Gaussian with a covariance [19]

$$\mathbf{\Sigma}_{j,k_G} = \text{blkdiag}\left(\sigma^2_{R_{j,k_G}}, \sigma^2_{\theta_{j,k_G}}, \sigma^2_{f_{j,k_G}}, \sigma^2_{\eta^R_{j,k_G}}, \sigma^2_{\eta^I_{j,k_G}}\right). \tag{14}$$

where $\sigma^2_{R_{j,k_G}}$, $\sigma^2_{\theta_{j,k_G}}$, $\sigma^2_{f_{j,k_G}}$, $\sigma^2_{h^R_{j,k_G}}$ and $\sigma^2_{h^I_{j,k_G}}$ are the CRLBs for the range, bearing, Doppler and RCS [4],[26] information

$$\begin{cases} \sigma^2_{R_{j,k_G}} \propto \left(\mu_{j,k_G}\beta_j^2\right)^{-1} \\ \sigma^2_{\theta_{j,k_G}} \propto \left(\mu_{j,k_G}/B_j\right)^{-1} \\ \sigma^2_{f_{j,k_G}} \propto \left(\mu_{j,k_G}E_j^2\right)^{-1} \\ \sigma^2_{h^R_{j,k_G}} = \sigma^2_{h^I_{j,k_G}} \propto \left(2\alpha_{j,k_G}P_{j,k_G}\right)^{-1} \end{cases} \tag{15}$$

In (15), $\alpha_{j,k_G} \propto 1/R^4_{j,k_G}$ is the attenuation parameter [4],[26] and

$$\mu_{j,k_G} \propto \alpha_{j,k_G}P_{j,k_G}\left|\boldsymbol{\eta}_{j,k_G}\right|^2 \tag{16}$$

is the *signal to noise ratio* (SNR). In (15), β_j and E_j are the signal effective bandwidth and effective time duration [4], respectively. B_j is the null to null beam width of the receiver antenna [26]. In (16), the operator $|\bullet|$ represents the 2-norm. Note that all the elements in (15) are inversely linear with the transmit power P_{j,k_G}, and thus the covariance can be written as

$$\mathbf{\Sigma}_{j,k_G} = P^{-1}_{j,k_G}\mathbf{Y}_{j,k_G} \tag{17}$$

Obviously, enhancing the transmit power of one radar will definitely increase its measurement accuracy.

III. Threshold Adjustment at Each Node

After we have the target state estimate $\boldsymbol{\xi}_{k_G-1|k_G-1}$ and the corresponding covariance $\mathbf{C}_{k_G-1|k_G-1}$, the target state, and the covariance matrix can be predicted as

$$\begin{cases} \boldsymbol{\xi}_{k_G|k_G-1} = \mathbf{F}\left(k_G, k_G-1\right)\boldsymbol{\xi}_{k_G-1|k_G-1} \\ \mathbf{C}_{k_G|k_G-1} = \mathbf{F}\left(k_G, k_G-1\right)\mathbf{C}_{k_G-1|k_G-1}\mathbf{F}^T\left(k_G, k_G-1\right) + \mathbf{Q}_\xi\left(k_G, k_G-1\right) \end{cases} \tag{18}$$

Moreover, we also have the predicted measurement and innovation covariance of radar j [27]

$$\begin{cases} \mathbf{z}_{j,k_G|k_G-1} = \mathbf{h}_j\left(\boldsymbol{\xi}_{k_G|k_G-1}\right) \\ \mathbf{S}_{j,k_G} = \mathbf{H}_{j,k_G}\mathbf{C}_{k_G|k_G-1}\mathbf{H}^T_{j,k_G} + \mathbf{\Sigma}_{j,k_G} \end{cases} \tag{19}$$

where $\mathbf{H}_{j,k_G} = \left[\Delta_{\xi_{k_G}}\mathbf{h}_j^T\left(\boldsymbol{\xi}_{k_G}\right)\right]^T$ is the $n_z \times \left(n_x + 2N\right)$ Jacobian matrix. From the Gaussian assumption, the validation gate of radar j can be drawn in Fig. 2, whose volume is (see Chap.10 in [27] for more detail)

$$V_{j,k_G} = c_{n_z} g^{\frac{n_z}{2}} \left|\mathbf{S}_{j,k_G}\right|^{\frac{1}{2}} \tag{20}$$

In (20), the coefficient c_{n_z} depends on the dimension of the measurement n_z [27], g is a constant controlling the size of validation region.

Suppose that radar j examines the echoes within its own validation gate to decide whether this target is present. Hence, a test of absence or presence of a target at location $\mathbf{z}^l_{j,k_G}$ is to be performed. Hypothesis H_0 is that there is no target at the l th test cell $\mathbf{z}^l_{j,k_G}$ and hence, the measured return is due simply to noise. Hypothesis H_1 is that there is indeed a target at location $\mathbf{z}^l_{j,k_G}$ and thus, the return is due to a combination of noise and signal energy.

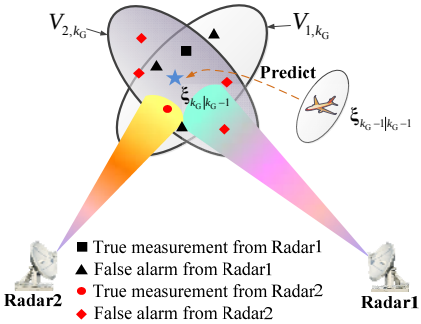

Fig. 2 The sketch map of the target measurement model

Commonly, a radar detector operates according to Neyman-Pearson (NP) criterion, and a fixed threshold is adopted. Our previous work [6] proved that, by appropriately using the prior track information within a cognitive manner, the detection performance may be efficiently enhanced. At each time index, the prior information available for radar j is [6][1]

$$\begin{cases} p_{\mathrm{H}_0}\left(\mathbf{z}^l_{j,k_G}\right) = 1/V_{j,k_G} \\ p_{\mathrm{H}_1}\left(\mathbf{z}^l_{j,k_G}\right) = \mathcal{N}\left(\mathbf{z}^l_{j,k_G}; \mathbf{h}_j\left(\boldsymbol{\xi}_{k_G|k_G-1}\right), \mathbf{H}_{j,k_G}\mathbf{C}_{k_G|k_G-1}\mathbf{H}^T_{j,k_G}\right) \\ \qquad\qquad = \mathcal{N}\left(\mathbf{z}^l_{j,k_G}; \mathbf{z}_{j,k_G|k_G-1}, \mathbf{D}_{j,k_G|k_G-1}\right) \end{cases} \tag{21}$$

Physically speaking, this feedback information is the predicted distribution of the target location, and from a practical point of view, the Bayesian threshold is then supposed to be depressed near where a target is expected to be and elevated where it is unexpected [11]. In this scenario, the averaged point FA over all the test cells can be calculated as [6]

$$P_{j,\mathrm{fa}} = \frac{1}{V_{j,k_G}}\left[\left(1+\mu_{j,k_G}\right)\chi^{\mathrm{BD}}_{j,k_G}\right]^{-\varsigma_{j,k_G}} \cdot \left[\frac{\sqrt{\varsigma_{j,k_G}}}{\sqrt{\left(2\pi\right)^{n_z}\left|\mathbf{\Sigma}_{j,k_G}\right|}}\right]^{\varsigma_{j,k_G}-1} \cdot \varsigma_{j,k_G}^{-\frac{\varsigma_{j,k_G}}{2}} \tag{22}$$

where $\chi^{\mathrm{BD}}_{j,k_G}$ is a constant which ensures the Bayesian detector operates with a desired FAR, and $\varsigma_{j,k_G} = \left(1+\mu_{j,k_G}\right)/\mu_{j,k_G}$ [6].

Constraining the FTR to be a required value, we can slightly decrease the detection threshold according to a predefined track confirmation rule [21] to improve the detection performance. In this paper, we consider a classical M_0-*of*-N_0 logic track confirmation rule [21]. Specifically, a target track will be confirmed if there exist M_0 measurements in the predicted region of N_0 successive frames.

To derive the relationship between the predefined FTR $P_{j,\mathrm{FTR}}$ and averaged point FA $P_{j,\mathrm{fa}}$, we first define a so-called frame false alarm rate $P_{j,\mathrm{Frame}}$, which denotes the probability

[1] A standard notation $\mathcal{N}\left(\mathbf{z};\mathbf{m},\mathbf{S}\right)$ is used in this paper to denote the Gaussian PDF of variable $\mathbf{z}$ with mean $\mathbf{m}$ and covariance matrix $\mathbf{S}$.

This article has been accepted for publication in a future issue of this journal, but has not been fully edited. Content may change prior to final publication. Citation information: DOI 10.1109/TSP.2017.2679693, IEEE Transactions on Signal Processing

that there exists at least one false alarm in the validation gate. With the assumption that the tests at different frames are mutually independent, the relationship between $P_{j,\mathrm{FTR}}$ and $P_{j,\mathrm{Frame}}$ can directly be obtained using Bernoulli formula

$$P_{j,\mathrm{FTR}} = \sum_{m=M_0}^{N_0} C_m^{N_0} P_{j,\mathrm{Frame}}^m \left(1-P_{j,\mathrm{Frame}}\right)^{N_0-m} \tag{23}$$

where

$$C_m^{N_0} = N_0!/\left[m!(N_0-m)!\right] \tag{24}$$

In radar applications, target detection for different test cells at one instant can also be assumed to be independent. Thus, the relationship between the frame false alarm rate $P_{j,\mathrm{Frame}}$ and the averaged point FAR in the predicted region is given by

$$P_{j,\mathrm{Frame}} = 1-\left(1-P_{j,\mathrm{fa}}\right)^{\psi_{k_\mathrm{G}}} \tag{25}$$

where ψ_{k_G} denotes the number of the test cells in the validation region. In (25), the term $\left(1-P_{j,\mathrm{fa}}\right)^{\psi_{k_\mathrm{G}}}$ actually denotes the probability that there exists no false alarm in one frame. In this scenario, for a given track confirmation rule and an acceptable FTR $P_{j,\mathrm{FTR}}$, the averaged FAR $P_{j,\mathrm{fa}}$ can be obtained through (23)-(25). Then, we can achieve $\chi_{j,k_\mathrm{G}}^{\mathrm{BD}}$ by using (22). Finally, we have the PD averaged over the validation gate as [6]

$$P_{\mathrm{d,BD}}^{j,k_\mathrm{G}} = \left[\frac{\left(1+\mu_{j,k_\mathrm{G}}\right)\chi_{j,k_\mathrm{G}}^{\mathrm{BD}}}{V_{j,k_\mathrm{G}}}\right]^{-\frac{1}{\mu_{j,k_\mathrm{G}}}} \cdot \left[\frac{\sqrt{\varsigma_{j,k_\mathrm{G}}}}{\sqrt{(2\pi)^{n_z}\left|\boldsymbol{\Sigma}_{j,k_\mathrm{G}}\right|}}\right]^{\varsigma_{j,k_\mathrm{G}}-1} \cdot \varsigma_{j,k_\mathrm{G}}^{-\frac{\varsigma_{j,k_\mathrm{G}}}{2}} \tag{26}$$

Herein, we have abused the notation somewhat: $P_{j,\mathrm{fa}}$ is the averaged point FA, $P_{\mathrm{d,BD}}^{j,k_\mathrm{G}}$ is the PD and P_{j,k_G} is the transmit power. Generally, the above derivations show that the closed-loop TA algorithm might be seen as an updated version of the works developed in [6] and [21]. In accordance with the two kinds of technical means introduced in Section I-B, the TA algorithm can either slightly decrease the detection threshold to enhance PD, or make full use of the feedback information to further facilitate target detection.

IV. Asynchronous Power Allocation Strategy

A. Basis of the Technique

Mathematically, the power allocation strategy can be formulated as a problem of optimizing a certain system level utility function subject to some resource constraints. In this paper, the adaptable parameters are the transmit power of different radars. However, in ARN, the sampling intervals of distinct radars are different, and thus it may not be appropriate for us to implement the power allocation strategy at each time index k_G. Instead of that, the APA strategy considered in this paper is carried out at time index $k_{\mathrm{AP},l}$, $l=1,2,\ldots L$ for the next period of time T_0, with

$$\begin{cases} t_{k_{\mathrm{AP},l+1}} = t_{k_{\mathrm{AP},l}} + T_0 \\ T_0 > T_i,\ \ i=1,\ldots,N \end{cases} \tag{27}$$

The second constraint implies that each radar at least generate one measurement during each allocation period. In this scenario, the measurements from different radars are sequentially assigned into different allocation periods, see Fig. 3 for detail.

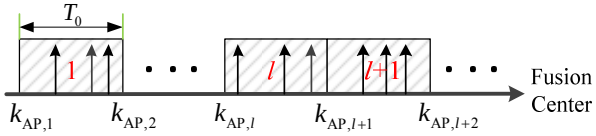

Fig. 3 The measurement assignment results in each allocation period

During the l th allocation period, the adaptable transmit power is of the following form

$$\mathbf{p}_l = \left[P_{1,l}, P_{2,l}, \ldots, P_{N,l}\right]^T \tag{28}$$

As references [7] and [17] state that, the *Bayesian information matrix* (BIM), whose inverse yields the BCRLB, bounds the error variance of the unbiased estimates of the target state, and thus is utilized as the optimization criterion for the APA strategy. During each allocation period (based on the obtained BIM at $k_{\mathrm{AP},l}$), we can analyze a set of candidates $\mathbf{p}_l$ and in each case determine a predicted BIM at time index $k_{\mathrm{AP},l+1}$, from which we can obtain the performance bounds. We are then in a position to design and control the transmit parameter in order to achieve better tracking performance.

B. Performance Metric for APA

For the l th allocation period, we assume that the measurements from different radars are sequentially indexed as $k_\mathrm{G},\ldots,k_\mathrm{G}+M_{l,k_\mathrm{G}}$

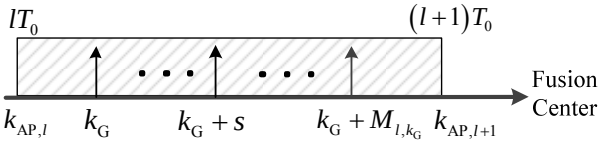

Fig. 4 The sampling model at the l th allocation period

According to Fig. 4, we see that, given the BIM $\mathbf{J}\left(\boldsymbol{\xi}_{k_{\mathrm{AP},l}}\right)$ and a candidate $\mathbf{p}_l$, the predicted BIM at time index $k_\mathrm{G}+M_{l,k_\mathrm{G}}$ needs to be recursively calculated $M_{l,k_\mathrm{G}}+1$ times as follows

$$\mathbf{J}\left(\boldsymbol{\xi}_{k_{\mathrm{AP},l}}\right) \to \mathbf{J}_{\boldsymbol{\xi}_{k_\mathrm{G}}}\left(\mathbf{p}_l\right) \to \cdots \to \mathbf{J}_{\boldsymbol{\xi}_{k_\mathrm{G}+M_{l,k_\mathrm{G}}}}\left(\mathbf{p}_l\right) \tag{29}$$

where $\mathbf{J}_{\boldsymbol{\xi}_{k_\mathrm{G}+s}}\left(\mathbf{p}_l\right)$ denotes the predicted BIM at time index $k_\mathrm{G}+s$, $s=0,\ldots,M_{l,k_\mathrm{G}}$. If we let $\mathbf{J}_{\boldsymbol{\xi}_{k_\mathrm{G}-1}}\left(\mathbf{p}_l\right)=\mathbf{J}\left(\boldsymbol{\xi}_{k_{\mathrm{AP},l}}\right)$, the BIM can be recursively and approximately calculated as follows (Here, we drop the expectation operator taken over the measurement Fisher information as [28])

$$\begin{aligned}\mathbf{J}_{\boldsymbol{\xi}_{k_\mathrm{G}+s}}\left(\mathbf{p}_l\right) = &\left[\mathbf{Q}_{\boldsymbol{\xi}}\left(k_\mathrm{G}+s,k_\mathrm{G}+s-1\right)+\mathbf{F}\left(k_\mathrm{G}+s,k_\mathrm{G}+s-1\right)\mathbf{J}_{\boldsymbol{\xi}_{k_\mathrm{G}+s-1}}^{-1}\left(\mathbf{p}_l\right)\mathbf{F}^T\left(k_\mathrm{G}+s,k_\mathrm{G}+s-1\right)\right]^{-1} \\ &+\sum_{j\in\mathbf{i}_{k_\mathrm{G}+s}}\left[\bar{\zeta}_{j,k_\mathrm{G}+s}P_{j,l}\bar{\mathbf{H}}_{j,k_\mathrm{G}+s}^T\mathbf{Y}_{j,k_\mathrm{G}+s}^{-1}\bar{\mathbf{H}}_{j,k_\mathrm{G}+s}\right]\end{aligned} \tag{30}$$

This article has been accepted for publication in a future issue of this journal, but has not been fully edited. Content may change prior to final publication. Citation information: DOI 10.1109/TSP.2017.2679693, IEEE Transactions on Signal Processing

In (30), $\bar{\zeta}_{j,k_G+s}$ is the *information reduction factor* (IRF), whose relationship with the target state can be determined off-line, prior to resource allocation [28]. $\bar{\mathbf{H}}_{j,k_G+s}$ is the Jacobian matrix evaluated at $\boldsymbol{\xi}_{k_G+s|k_G+s-1}$, where $\boldsymbol{\xi}_{k_G+s|k_G+s-1}$ denotes the predicted state vector for the case of zero process noise [19].

Finally, the predicted BIM for the l th allocation period can be obtained as follows

$$\begin{aligned}\mathbf{J}_{\xi_{k_{\mathrm{AP},l+1}}}(\mathbf{p}_l)=&\Big[\mathbf{Q}_{\xi}\left(k_{\mathrm{AP},l+1},k_G+M_{l,k_G}\right)\\&+\mathbf{F}\left(k_{\mathrm{AP},l+1},k_G+M_{l,k_G}\right)\mathbf{J}^{-1}_{\xi_{k_G+M_{l,k_G}}}(\mathbf{p}_l)\mathbf{F}^T\left(k_{\mathrm{AP},l+1},k_G+M_{l,k_G}\right)\Big]^{-1}\end{aligned} \tag{31}$$

The predicted BCRLB of the target is defined as the inverse of the predicted BIM:

$$\mathbf{C}^{\mathrm{CRLB}}_{\xi_{k_{\mathrm{AP},l+1}}}(\mathbf{p}_l)=\mathbf{J}^{-1}_{\xi_{k_{\mathrm{AP},l+1}}}(\mathbf{p}_l) \tag{32}$$

The diagonal elements of $\mathbf{C}^{\mathrm{CRLB}}_{\xi_{k_{\mathrm{AP},l+1}}}(\mathbf{p}_l)$ denote the lower bound on the variances of the estimation of the hybrid target state at the l th allocation period.

Conventional resource allocation techniques use the trace of the BCRLB as the optimization criterion [7],[17],[28]. However, the elements of the BCRLB matrix are at different scales, and thus it is intuitive for us to normalize the BCRLB and rewrite the criterion as follows

$$\mathbb{F}(\mathbf{p}_l)=\sqrt{\mathrm{Tr}_{n_{\mathbf{x}}}\left(\mathbf{\Lambda}\mathbf{C}^{\mathrm{CRLB}}_{\xi_{k_{\mathrm{AP},l+1}}}(\mathbf{p}_l)\mathbf{\Lambda}^T\right)} \tag{33}$$

where

$$\mathbf{\Lambda}=\mathrm{blkdiag}\left(\mathbf{I}_2\otimes\begin{bmatrix}1&0\\0&T_0\end{bmatrix},\mathbf{I}_{2N}\right) \tag{34}$$

is the normalization matrix, and $\mathrm{Tr}_n(\mathbf{A})$ returns the sum of the former n diagonal elements of matrix $\mathbf{A}$.

C. Criterion Minimization Technique

For a given total power budget P_{total} in each allocation period, the aim of our work is to optimally allocate the power resource which can result in the minimization of the predicted BCRLB based on the criterion (33). In such a model, the resource utilization efficiency can evidently be improved. The resulting optimization problem at the l th allocation period is:

$$\begin{aligned}&\min_{\mathbf{p}_l}\left(\mathbb{F}(\mathbf{p}_l)\right)\\ s.t.\quad&P_{i,l}-\bar{P}_{i\min}\ge 0\quad i=1,..,N\\&-P_{i,l}+\bar{P}_{i\max}\ge 0\\&\mathbf{1}_N^T\mathbf{p}_l=P_{\mathrm{total}}\end{aligned} \tag{35}$$

The former two constraints imply that the transmit power of each radar is constrained by a minimum and maximum value, while the last one represents that the transmit power of all the radars is limited in each allocation period. The intractability of this problem basically comes from the objective function, as: (a) the BCRLB needs to be recursively calculated $M_{l,k_G}+2$ times; (b) the IRF $\bar{\zeta}_{j,k_G+s}$ is highly nonlinear with respect to $\mathbf{p}_l$ [28]; Therefore, the optimization problem in (35) is nonlinear and nonconvex with respect to the power vector $\mathbf{p}_l$. To solve this problem, we first choose an appropriate relaxation of the objective function, and then use the optimal solution as a start point to find a constrained stationary point for the original problem (35). In this scenario, we find an approximate, convex formulation of the problem by replacing $\mathbb{F}(\mathbf{p}_l)$ as $\mathbb{S}(\mathbf{p}_l)$

$$\mathbb{S}(\mathbf{p}_l)=\sqrt{\mathrm{Tr}_{n_{\mathbf{x}}}\left(\mathbf{\Lambda}\mathbf{C}^{\text{R-CRLB}}_{\xi_{k_{\mathrm{AP},l+1}}}(\mathbf{p}_l)\mathbf{\Lambda}^T\right)} \tag{36}$$

In (36), $\mathbf{C}^{\text{R-CRLB}}_{\xi_{k_{\mathrm{AP},l+1}}}(\mathbf{p}_l)=\left[\mathbf{J}^{\text{R-CRLB}}_{\xi_{k_{\mathrm{AP},l+1}}}(\mathbf{p}_l)\right]^{-1}$ is the *relaxed BCRLB* (R-BCRLB) of the l th allocation period, and

$$\begin{aligned}\mathbf{J}^{\text{R-CRLB}}_{\xi_{k_{\mathrm{AP},l+1}}}(\mathbf{P}_l)=&\Big[\mathbf{Q}_{\xi}\left(k_{\mathrm{AP},l+1},k_{\mathrm{AP},l}\right)+\mathbf{F}\left(k_{\mathrm{AP},l+1},k_{\mathrm{AP},l}\right)\mathbf{J}^{-1}\left(\xi_{k_{\mathrm{AP},l}}\right)\mathbf{F}^T\left(k_{\mathrm{AP},l+1},k_{\mathrm{AP},l}\right)\Big]^{-1}\\&+\sum_{s=0}^{M_{l,k_G}}\sum_{j\in\mathbf{i}_{k_G+s}}\left[P_{j,l}\bar{\mathbf{H}}^T_{j,k_G+s}\mathbf{Y}^{-1}_{j,k_G+s}\bar{\mathbf{H}}_{j,k_G+s}\right]\end{aligned} \tag{37}$$

is the *relaxed BIM* (R-BIM). On one hand, as the IRF satisfies $\bar{\zeta}_{j,k_G+s}\in[0,1]$ [29], and is a monotonic increasing function of $P_{j,l}$, thus, we relax the original problem by dropping the IRF off. On the other hand, to avoid recursion, we calculate the R-BIM as (37), whose relationship with (31) can be found in Appendix A. Physically speaking, the first term on the right side of (37) characterizes the target motion information, and the latter term denotes the total measurement information provided by multiple radars during the l th allocation period. Thus, the R-BIM is the same as the BIM calculated for the synchronized scenario [7], in which all the measurements from different radar during the l th allocation period are assumed to be obtained at time index $k_{\mathrm{AP},l+1}$. Therefore, we know that the solution to the relaxed problem may provide a reasonable start point for the original problem in (35). An intuitive explanation is that the radars with better angular spread and closer distance will always be assigned with more power resource in both synchronous and asynchronous case. Here, the relaxed optimization problem is written as

$$\begin{aligned}&\min_{\mathbf{p}_l}\left(\mathbb{S}(\mathbf{p}_l)\right)\\ s.t.\quad&P_{i,l}-\bar{P}_{i\min}\ge 0\quad i=1,..,N\\&-P_{i,l}+\bar{P}_{i\max}\ge 0\\&\mathbf{1}_N^T\mathbf{p}_l=P_{\mathrm{total}}\end{aligned} \tag{38}$$

The optimization problem described in (38) is convex (the valid proof is given in Appendix B). Thus, the exact solution $\tilde{\mathbf{p}}_{l,\mathrm{opt}}$ can be obtained using convex optimization tools [30]. After that, this optimal solution $\tilde{\mathbf{p}}_{l,\mathrm{opt}}$ is utilized as the start point for a local optimization, applied to the nonconvex problem in (35). Here, we use the SPG algorithm to search for a suboptimal allocation results $\mathbf{p}_{l,\mathrm{opt}}$ [22]. The SPG algorithm is an extension of classical gradient projection method, which includes a nonmonotone line search strategy to accelerate the algorithm with guaranteed convergence [22]. The detailed steps of the SPG algorithm are given in Table I, in which $\Delta_{\mathbf{p}_{l,j}}\mathbb{F}(\mathbf{p}_{l,j})$ is first derivative of the objective function, with respect to $\mathbf{p}_{l,j}$.

TABLE I. THE SPG ALGORITHM

This article has been accepted for publication in a future issue of this journal, but has not been fully edited. Content may change prior to final publication. Citation information: DOI 10.1109/TSP.2017.2679693, IEEE Transactions on Signal Processing

Step(1) Choose a feasible point as $\mathbf{p}_{l,0}=\tilde{\mathbf{p}}_{l,\text{opt}}$. Initialize the iteration index $j=0$, the step length $\lambda_j=1$, and the stopping threshold ε. Set the parameter $\alpha_j\in[\alpha_{\min},\alpha_{\max}]$ as [22];

Step(2) Compute the spectral projected gradient as $\mathbf{d}_j=\Pr\left(\mathbf{p}_{l,j}-\alpha_j\Delta_{\mathbf{p}_{l,j}}\mathbb{F}\left(\mathbf{p}_{l,j}\right)\right)-\mathbf{p}_{l,j}$ [22], where $\Pr(\bullet)$ is the orthogonal projection operator;

Step(3) Adjust the step length λ_j and the parameter α_j the according to reference [22];

Step(4) Update the power vector $\mathbf{p}_{l,j+1}=\mathbf{p}_{l,j}+\lambda_j\mathbf{d}_j$

Step(5) If $\left|\Pr\left(\mathbf{p}_{l,j}-\alpha_j\Delta_{\mathbf{p}_{l,j}}\mathbb{F}\left(\mathbf{p}_{l,j}\right)\right)-\mathbf{p}_{l,j}\right|<\varepsilon$, $\mathbf{p}_{l,\text{opt}}=\mathbf{p}_{l,j+1}$, stop; Else $j=j+1$, go to Step(2).

D. Target State Estimation

After we have the optimized result $\mathbf{p}_{l,\text{opt}}$ for each allocation period, we adopt the JDTP algorithm derived in [6] to estimate the target state at each time index k_{G}. The basic diagram of the closed-loop JTAPA algorithm can be summarized as Fig. 5.

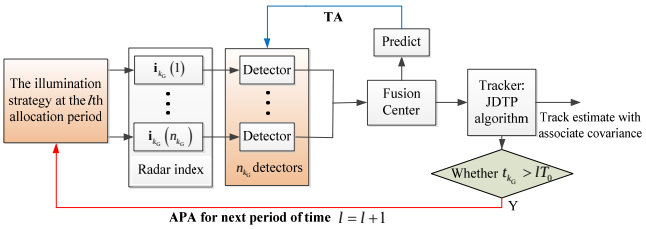

Fig. 5 System model of the closed-loop JTAPA scheme

In the following, the detailed steps of the closed-loop JTAPA algorithm are summarized in Table II for cognitive target tracking in ARN, according to which we can recursively achieve the target state $\boldsymbol{\xi}_{k_{\text{G}}|k_{\text{G}}}$ and the corresponding covariance matrix $\mathbf{C}_{k_{\text{G}}|k_{\text{G}}}$ at each time index.

TABLE II. THE STEPS OF THE CLOSED-LOOP JTAPA ALGORITHM

Step(1) Let $l=1$, $k_{\text{AP},l}=0$, initiate $\boldsymbol{\xi}_{k_{\text{AP},l}|k_{\text{AP},l}}$, $\mathbf{C}_{k_{\text{AP},l}|k_{\text{AP},l}}=\mathbf{J}^{-1}\left(\boldsymbol{\xi}_{k_{\text{AP},l}}\right)$;

Step(2) Calculate the criterion $\mathbb{F}\left(\mathbf{p}_l\right)$ according to (31)-(33), and implement the APA strategy for the l th allocation period (detailed in Section IV-C);

Step(3) Send the allocation result $\mathbf{p}_{l,\text{opt}}$ to the ARN to form the illumination strategy during the l th allocation period;

Step (4) In the l th allocation period, there exist a number of $M_{l,k_{\text{G}}}+1$ sampling indices. Let $\mathbf{C}_{k_{\text{G}}-1|k_{\text{G}}-1}=\mathbf{C}_{k_{\text{AP},l}|k_{\text{AP},l}}$, and then for $s=0,\ldots M_{l,k_{\text{G}}}$

(4.1) Predict the target state, the measurements and the covariance matrix according to (18) and (19) for $j\in\mathbf{i}_{k_{\text{G}}+s}$;

(4.2) Define the track confirmation rule, and calculate $P_{j,\text{fa}}$ according (23) and (25). Then, we can obtain $\chi_{j,k_{\text{G}}}^{\text{BD}}$ and $P_{\text{d,BD}}^{j,k_{\text{G}}+s}$, as well as the detection threshold, through (22) and (26). In this case, the thresholded measurement collected from different radar at time index $k_{\text{G}}+s$ can be visualized as

$$\mathbf{Z}_{k_{\text{G}}+s}\to\left[\cdots,\left\{0,1,\ldots,m_{j,k_{\text{G}}+s}\right\},\cdots\right]^T,\ j\in\mathbf{i}_{k_{\text{G}}+s}$$

(4.3) Calculate the association probability. Here, we assume that Π_k^J is a 'joint' event corresponding to unique permutation of measurement from different radar [6]. For the J th association event, the association probability is [6]

$$\beta_{k_{\text{G}}+s}^J\triangleq p\left\{\Pi_{k_{\text{G}}+s}^J\middle|\mathbf{Z}_{k_{\text{G}}+s}\right\},$$

As the measurement errors of different radars are independent from one another, the joint association probability can be calculated as

$$\beta_{k_{\text{G}}+s}^J\triangleq\prod_{j=1}^{n_{k_{\text{G}}+s}}p\left\{\pi_{\mathbf{i}_{k_{\text{G}}+s}(j),k_{\text{G}}+s}^{J(j)}\middle|\mathbf{Z}_{\mathbf{i}_{k_{\text{G}}+s}(j),k_{\text{G}}+s}\right\}$$

where $\pi_{\mathbf{i}_{k_{\text{G}}+s}(j),k}^{J(j)}$ denotes the event that the $J(j)$ th measurement of radar station $\mathbf{i}_{k_{\text{G}}+s}(j)$ is correct. $J(j)=0$ represents the event that none of the measurements of the radar $\mathbf{i}_{k_{\text{G}}+s}(j)$ is correct. $p\left\{\pi_{\mathbf{i}_{k_{\text{G}}+s}(j),k_{\text{G}}+s}^{J(j)}\middle|\mathbf{Z}_{\mathbf{i}_{k_{\text{G}}+s}(j),k_{\text{G}}+s}\right\}$ is the association probability of a single radar [6].

(4.4) State update

$$\boldsymbol{\xi}_{k_{\text{G}}+s|k_{\text{G}}+s}=\sum_J\boldsymbol{\xi}_{J,k_{\text{G}}+s|k_{\text{G}}+s}\beta_{k_{\text{G}}+s}^J.$$

The number of the association events J is defined as

$$N_{k_{\text{G}}+s}=\prod_{j=1}^{n_{k_{\text{G}}}}\left(C_1^{m_{\mathbf{i}_{k_{\text{G}}+s}(j),k_{\text{G}}+s}}+C_0^{m_{\mathbf{i}_{k_{\text{G}}+s}(j),k_{\text{G}}+s}}\right).$$

and $\boldsymbol{\xi}_{J,k|k}$ is the updated state conditioned on the J th event

$$\boldsymbol{\xi}_{J,k_{\text{G}}+s|k_{\text{G}}+s}=\boldsymbol{\xi}_{k_{\text{G}}+s|k_{\text{G}}+s-1}+\sum_{j=1}^{n_{k_{\text{G}}+s}}\mathbf{K}_{\mathbf{i}_{k_{\text{G}}+s}(j),k_{\text{G}}+s}^{J(j)}\mathbf{v}_{\mathbf{i}_{k_{\text{G}}+s}(j),k_{\text{G}}+s}^{J(j)}.$$

$\mathbf{v}_{\mathbf{i}_{k_{\text{G}}+s}(j),k_{\text{G}}+s}^{J(j)}$ is the corresponding innovation, and $\mathbf{K}_{\mathbf{i}_{k_{\text{G}}+s}(j),k_{\text{G}}+s}^{J(j)}$ is the gain [27].

(4.5) Covariance update

$$\mathbf{C}_{k_{\text{G}}+s|k_{\text{G}}+s}=\sum_J\beta_{k_{\text{G}}+s}^J\left[\mathbf{C}_{J,k_{\text{G}}+s|k_{\text{G}}+s}+\boldsymbol{\xi}_{J,k_{\text{G}}+s|k_{\text{G}}+s}\left(\boldsymbol{\xi}_{J,k_{\text{G}}+s|k_{\text{G}}+s}\right)^T\right]-\boldsymbol{\xi}_{k_{\text{G}}+s|k_{\text{G}}+s}\left(\boldsymbol{\xi}_{k_{\text{G}}+s|k_{\text{G}}+s}\right)^T$$

where $\mathbf{C}_{J,k_{\text{G}}+s|k_{\text{G}}+s}$ is the individual covariance corresponding to $\boldsymbol{\xi}_{J,k_{\text{G}}+s|k_{\text{G}}+s}$ [27].

(4.6) Let $s=s+1$, and go to Step(4).

Step(5) Calculate the initial state and covariance for the next allocation period

$$\begin{cases}\boldsymbol{\xi}_{k_{\text{AP},l+1}|k_{\text{AP},l+1}}=\mathbf{F}\left(k_{\text{AP},l+1},k_{\text{G}}+M_{l,k_{\text{G}}}\right)\boldsymbol{\xi}_{k_{\text{G}}+M_{l,k_{\text{G}}}|k_{\text{G}}+M_{l,k_{\text{G}}}}\\ \mathbf{C}_{k_{\text{AP},l+1}|k_{\text{AP},l+1}}=\mathbf{Q}_{\xi}\left(k_{\text{AP},l+1},k_{\text{G}}+M_{l,k_{\text{G}}}\right)+\\ \qquad\mathbf{F}\left(k_{\text{AP},l+1},k_{\text{G}}+M_{l,k_{\text{G}}}\right)\mathbf{C}_{k_{\text{G}}+M_{l,k_{\text{G}}}|k_{\text{G}}+M_{l,k_{\text{G}}}}\mathbf{F}^T\left(k_{\text{AP},l+1},k_{\text{G}}+M_{l,k_{\text{G}}}\right)\end{cases}$$

let $l=l+1$, and then go to Step(2);

V. SIMULATION RESULTS

In this section, an ARN with $N=4$ spatially diverse radars is considered. We assume that the initial sampling time instants of different radars are the same. The null to null beam width of each radar's receiver is $B_i=5$ m, and the signal effective bandwidth and effective time duration of each radar are set as $\beta_i=1$ MHz and $E_i=1$ ms, respectively. Some other radar working parameters are listed in Table III.

TABLE III. THE WORKING PARAMETERS OF EACH RADAR

Radar index	$i=1$	$i=2$	$i=3$	$i=4$
(x_i,y_i) /km	$(0,-60)$	$(70,0)$	$(-70,0)$	$(-62,0)$
$f_{c,i}$ /GHz	1	1.01	1.02	1.03

We also assume that a single target is initially located at $(0,0)$ km, and moves with a constant speed of $(-80,-100)$ m/s, and then its measurements with a time length of $T_{\text{G}}=60$

This article has been accepted for publication in a future issue of this journal, but has not been fully edited. Content may change prior to final publication. Citation information: DOI 10.1109/TSP.2017.2679693, IEEE Transactions on Signal Processing

seconds is used to support our simulation. The angular spread of the target trajectory with respect to the ARN is as follows.

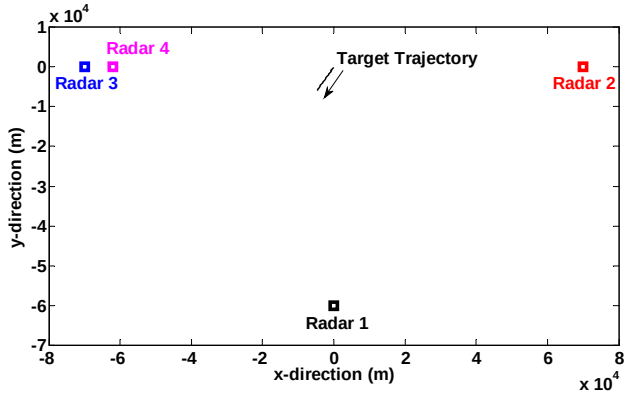

Fig. 6 Deployment of target with respect to the ARN

In our simulation, the FTR of each radar is set as $P_{j,\mathrm{FTR}}=10^{-8}$, and the track confirmation rule is defined as the M_0-*of*-N_0 logic, where $M_0=3$, and $N_0=5$. In this scenario, the frame false alarm rate is calculated by (23) as $P_{j,\mathrm{Frame}}\approx 10^{-3}$, and the averaged FAR $P_{j,\mathrm{fa}}$ can be obtained through (25). The gate size parameter is $g=8$, and the lower and upper bounds of the power of each radar are set as $\overline{P}_{i\min}=0.01P_{\mathrm{total}}$, $\overline{P}_{i\max}=0.8P_{\mathrm{total}}$, respectively. The initial SNR is set as $\mu_0=10$ dB for $R_0=60$ km with target RCS equals 1.

In order to better reveal the effects of several factors on the power allocation results, we consider two RCS models ($\boldsymbol{\eta}_1$, $\boldsymbol{\eta}_2$). For simplicity, we set

$$\boldsymbol{\eta}_1:\begin{cases}\left[\eta^R_{1,1},\ldots,\eta^R_{i,k_G},\ldots,\eta^R_{N,K_G}\right]^T=\mathbf{1}^T_{NK_G}\\ \left[\eta^I_{1,1},\ldots,\eta^I_{i,k_G},\ldots,\eta^I_{N,K_G}\right]^T=\mathbf{0}^T_{NK_G}\end{cases}\tag{39}$$

where K_G denotes the number of the global sampling instants. This case supports the evaluation of the resource allocation strategy with the target RCS factored out. In the second RCS model $\boldsymbol{\eta}_2$, the real parts of the target reflectivity with respect to radar 1 and radar 2 are set as Fig. 7, while other RCS parameters are kept the same as $\boldsymbol{\eta}_1$.

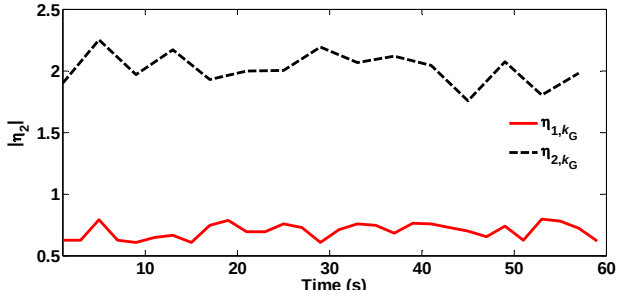

Fig. 7 The second RCS model $\boldsymbol{\eta}_2$

Moreover, to evaluate the influence of the sampling frequencies on the allocation results, we also consider two sampling models ($\mathbf{t}_1$, $\mathbf{t}_2$), as is shown in Table IV. Given the time length $T_G=60$ and the allocation interval $T_0=5$, the total number of the allocation periods is $L=T_G/T_0=12$, while the two sampling models will result in different measurement models in each allocation period.

TABLE IV. TWO SAMPLING MODELS

$\mathbf{t}_1$	$T_1=2$ s	$T_2=4$ s	$T_3=2.5$ s	$T_4=5$ s
$\mathbf{t}_2$	$T_1=4$ s	$T_2=2.5$ s	$T_3=2.5$ s	$T_4=2.5$ s

Combining these different target RCS models and sampling models, we investigate the following three cases, and our simulations are implemented with the following two goals: (a) Show the enhancement of the tracking accuracy brought by the JTAPA strategy; (b) Reveal the effects of several factors on the allocation results.

A. *Case* 1: $\boldsymbol{\eta}_1$ *and* $\mathbf{t}_1$

This case supports the evaluation of the JTAPA strategy with the target RCS factored out. To better examine the optimality of the proposed method, the position tracking *root mean square error* (RMSE) achieved with the JTAPA strategy, as well as the corresponding BCRLB, are used as a metric to compare with two benchmarks

$$\mathrm{RMSE}_{k_G}=\frac{1}{N_{MC}}\sum_{j=1}^{N_{MC}}\left[\left(x_{\mathrm{T}k_G}-\hat{x}^j_{\mathrm{T}k_G}\right)^2+\left(y_{\mathrm{T}k_G}-\hat{y}^j_{\mathrm{T}k_G}\right)^2\right]\tag{40}$$

where N_{MC} is the number of the Monte Carlo trials, $\left(\hat{x}^j_{\mathrm{T}k_G},\hat{y}^j_{\mathrm{T}k_G}\right)$ is target state estimate at the jth trial. The first benchmark implies that each radar operates according to NP criterion with $P_{j,\mathrm{fa}}=10^{-6}$, while the second one adopts a NP detector with a FAR the same as the JTAPA strategy. In both benchmarks, the limited power budget in each allocation period is uniformly allocated to multiple radars as $\mathbf{p}_{I,0}=P_{\mathrm{total}}/N\cdot\mathbf{1}^T_N$. Benchmark 1 is used to verify the superiority of the JTAPA strategy, with respect to the traditional multistatic tracking method with an empirical FAR, while benchmark 2 is utilized to show the enhancement brought by TA (Bayesian detection) and APA processes under a fair FAR condition.

For the first sampling model $\mathbf{t}_1$, the number of the global tracking instants is $K_G=48$. Overall speaking, the closed-loop JTAPA algorithm can markedly improve the tracking accuracy by using the TA and APA processes with a fair FAR condition, and decreasing the threshold of each radar according to a predefined track confirmation rule can further enhance the tracking performance. It is noteworthy that, for different global time indices, the origination and the number of the measurements ($\mathbf{i}_{k_G}$ and n_{k_G}) are different. Therefore, the tracking BCRLBs and the RMSEs are not smooth in Fig. 8.

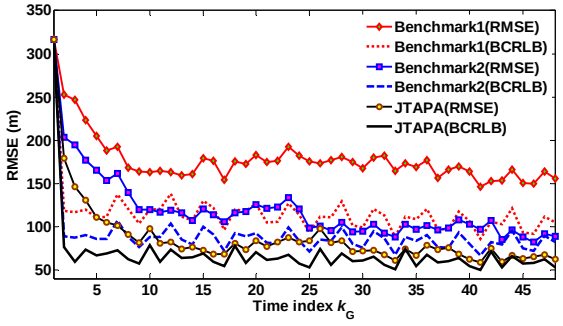

Fig. 8 The position tracking performance in case 1

To separately determine the contributions of the TA and the

This article has been accepted for publication in a future issue of this journal, but has not been fully edited. Content may change prior to final publication. Citation information: DOI 10.1109/TSP.2017.2679693, IEEE Transactions on Signal Processing

APA processes under a fair FAR condition, Fig. 9 shows the performance enhancement achieved with different initial SNR μ_0 for case 1. Herein, the performance enhancement is defined as the percentage of the improved tracking accuracy, with respect to the results achieved with the parameters of benchmark 2

$$\Gamma(\mu_0)=1-\frac{\sum_{k_G}\mathrm{Tr}\left(\mathbf{J}_{\xi_{k_G}}^{-1}\left(P_{\mathrm{d,BD}}^{j,k_G},\mathbf{p}_{l,\mathrm{opt}},\mu_0\right)\right)}{\sum_{k_G}\mathrm{Tr}\left(\mathbf{J}_{\xi_{k_G}}^{-1}\left(P_{\mathrm{d,NP}}^{j,k_G},\mathbf{p}_{l,0},\mu_0\right)\right)} \tag{41}$$

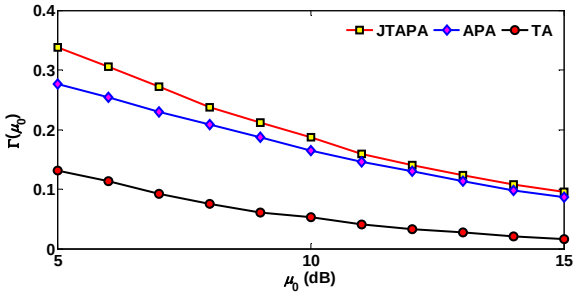

Fig. 9 The percentage of the improved tracking accuracy in case 1

The results in Fig. 9 suggest that the APA strategy generally introduces larger gain in tracking accuracy than the TA process (without decreasing the threshold), and the integration of the TA and APA processes may further improve the tracking performance. The results also yield that the proposed JTAPA algorithm is more preferable in low SNR case, as there exists less chance of promotions in both the detection probability and the IRF for the high SNR case.

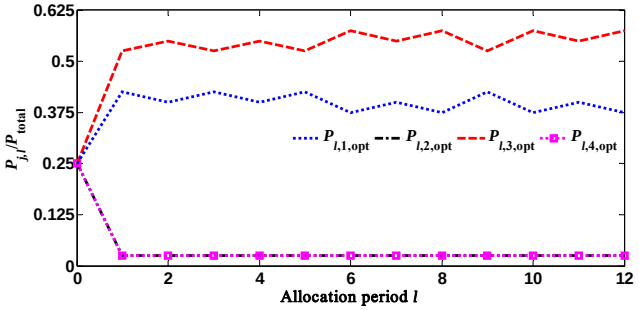

Fig. 10 Power allocation results in each allocation period for case 1

In order to disclose the effects of several factors on the allocation results, the power assignment results for each allocation period are shown in Fig. 10 for case 1. At the initial allocation index $l=0$, there exists no prior information, and thus the limited power resource is uniformly allocated to different radars. For $k>1$, the allocation results are different from the synchronous case, in which the transmit power is assigned to the radars closer to the target [7]. More power is assigned to radar 1 and radar 3, as the sampling frequencies of these radars are higher. An intuitive explanation is that, these two radars are likely to generate more measurements in each allocation period, when compared with the remaining radars. Therefore, distributing more power resource to these two radars may better improve the tracking performance. Moreover, in accordance with our previous finding in [7], we see from Fig. 10 that, among the two selected radars, higher power is assigned to the radars with relative larger distance (radar 3 in this case).

B. *Case* 2: $\boldsymbol{\eta}_2$ *and* $\mathbf{t}_1$

We then expand our simulation while considering the loss due to the target RCS by using $\boldsymbol{\eta}_2$. The tracking performance is evaluated in Fig. 11 for the second case. The results prove that the JTAPA algorithm may make more complete use of the prior information of the ARN to implement TA and APA, and thus can achieve better tracking performance.

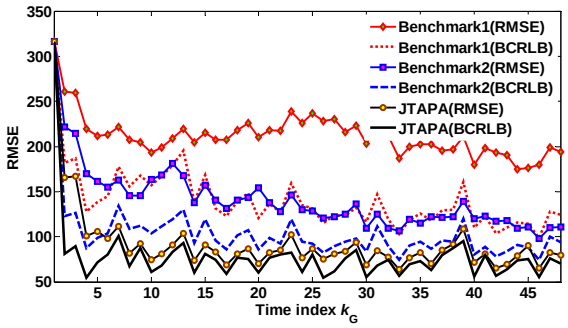

Fig. 11 The position tracking performance in case 2

In Fig. 12, the performance enhancement achieved with different initial SNR μ_0 is given for case 2 under a fair FAR condition. Similar to case 1, the results also show that both the TA and the APA can improve target tracking accuracy, and the improvements increase as the decreasing of the SNR. In this scenario, we may conclude that the superiority of the JTAPA algorithm can better be expressed in the low SNR case.

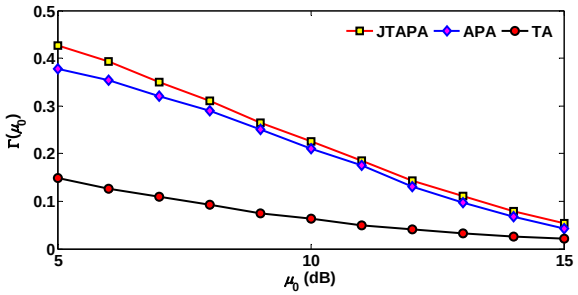

Fig. 12 The percentage of the improved tracking accuracy in case 2

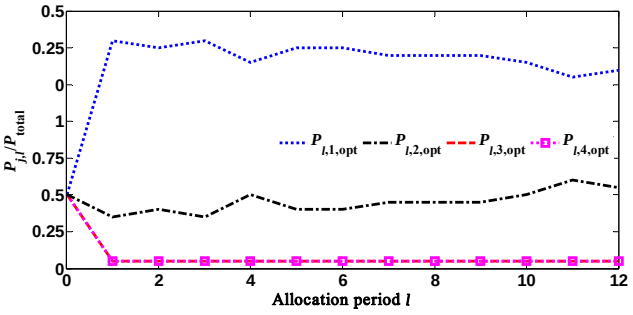

Fig. 13 Power allocation results in each allocation period for case 2

The power allocation results for case 2 are presented in Fig .13. In this case, although radar 3 benefits from higher sampling frequency, more power is allocated to radar 2, based on the fact that radar 2 has better reflectivity condition.

This article has been accepted for publication in a future issue of this journal, but has not been fully edited. Content may change prior to final publication. Citation information: DOI 10.1109/TSP.2017.2679693, IEEE Transactions on Signal Processing

According to Fig. 6, we know that radar 1 has better angular spread than other radars, and thus it must play a significant role in the illumination strategy, disregarding its channel disadvantage. Therefore, more power resource is distributed to radar 1 and radar 2. Among those two radars, higher power is assigned to the radar with relative weaker propagation path (radar 1 in this case), see Fig. 13 for detail.

C. *Case* 3: $\boldsymbol{\eta}_1$ *and* $\mathbf{t}_2$

In this part, we analyze the effect of the sampling interval T_i on the allocation results. In this case, the number of the global tracking instants for $\mathbf{t}_2$ is $K_G = 36$. The tracking performance is given in Fig. 14 for this case, from which we see the superiority of the proposed JTAPA strategy.

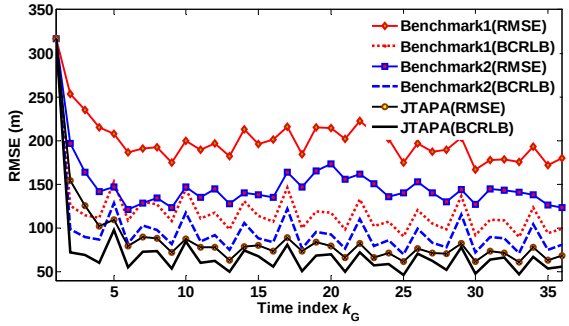

Fig. 14 The position tracking performance in case 3

In Fig. 15, the contributions of the TA and APA strategies are separately considered for case 3, according to which we see that the performance gain achieved with the APA process is larger than that obtained with the TA strategy with a fair FAR condition.

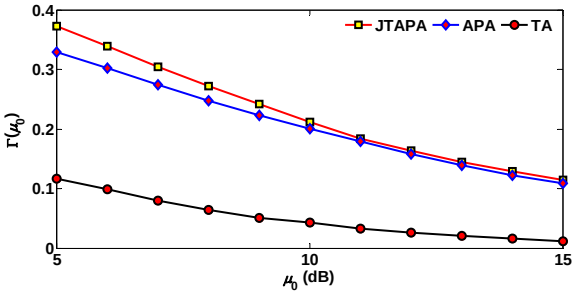

Fig. 15 The percentage of the improved tracking accuracy in case 3

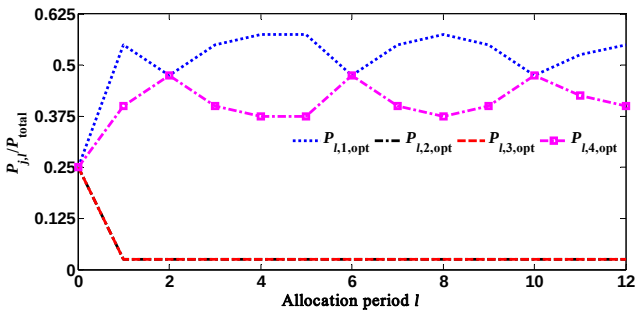

Fig. 16 Power allocation results in each allocation period for case 3

The relationship between the sampling interval T_i and the power allocation result is highlighted in Fig. 16 for case 3. On one hand, rather than using the radar with higher sampling frequency as case 1, radar 1, which has an irreplaceable deployment with respect to other radars, is assigned with more power. On the other hand, radar 4 is designated to cooperate with radar 1 to track the target, as it has better observe condition than other radars (the target is moving toward radar 4).

From Fig. 8 to Fig. 16, it can be seen that the open-loop tracking method generally exhibits higher tracking RMSE, compared with the proposed JTAPA algorithm. The results also imply that the JTAPA algorithm can enhance the detection performance, increase the resource utilization efficiency of the ARN, and remarkably improve the target tracking accuracy with a given power budget. In the power optimization process, higher power tends to allocated to the radars with better observation and reflectivity conditions, as well as higher sampling frequencies, such that the tracking accuracy can better be improved.

VI. Conclusion

A closed-loop JTAPA algorithm is developed for cognitive target tracking in ARN. The basis of this algorithm is to adjust the detection threshold and optimize the power assignment by properly using the feedback information. On one hand, the detectors use the information about the target location to set a Bayesian detection threshold, while constraining the FTR to be a required value. On the other hand, the BCRLB is derived, normalized and utilized as an objective function for the APA process. Then, the resulting optimization problem is solved through relaxation incorporating the SPG technique. Simulation results demonstrate that the APA strategy may introduce larger gain in tracking accuracy than the TA process under a fair FAR condition, and the integration of the TA and APA processes may further improve the tracking performance. The deviation shows that the proposed JTAPA strategy can easily be generalized to the distributed MIMO radar case (consists of M transmitting and N receiving radars), as this case is equivalent to the netted monostatic case with MN radars. In the future, we will consider the multiple target tracking case, and validate the correctness of the proposed JTAPA algorithm using real data.

Appendix A

The relationship between (31) and (37)

According to (30), if we let $\mathbf{J}^1_{\xi_{k_G-1}} = \mathbf{J}\left(\boldsymbol{\xi}_{k_{AP,l}}\right)$ and $\mathbf{J}^2_{\xi_{k_G-1}} = \mathbf{0}$, the BIM at time index $k_G + s$ can be written compactly as

$$\mathbf{J}_{\xi_{k_G+s}}\left(\mathbf{p}_l\right) = \mathbf{J}^1_{\xi_{k_G+s}} + \mathbf{J}^2_{\xi_{k_G+s}}, \tag{42}$$

where $\mathbf{J}^1_{\xi_{k_G+s}}$ and $\mathbf{J}^2_{\xi_{k_G+s}}$ denotes the target motion and measurement information matrix at time index $k_G + s$

$$\begin{cases} \mathbf{J}^1_{\xi_{k_G+s}} = \Big[\mathbf{Q}_\xi\left(k_G+s, k_G+s-1\right) + \\ \qquad \mathbf{F}\left(k_G+s, k_G+s-1\right)\left(\mathbf{J}^1_{\xi_{k_G+s-1}} + \mathbf{J}^2_{\xi_{k_G+s-1}}\right)^{-1}\mathbf{F}^T\left(k_G+s, k_G+s-1\right)\Big]^{-1} \\ \mathbf{J}^2_{\xi_{k_G+s}} = \sum_{j\in\mathbf{i}_{k_G+s}}\left[\bar{\zeta}_{j,k_G+s} P_{j,l}\bar{\mathbf{H}}^T_{j,k_G+s}\mathbf{Y}^{-1}_{j,k_G+s}\bar{\mathbf{H}}_{j,k_G+s}\right] \end{cases} \tag{43}$$

This article has been accepted for publication in a future issue of this journal, but has not been fully edited. Content may change prior to final publication. Citation information: DOI 10.1109/TSP.2017.2679693, IEEE Transactions on Signal Processing

As the IRF is a monotonic increasing function of $P_{j,l}$, we relax the original problem by dropping the IRF off. In this scenario, the relaxed measurement information gathered by multiple radars at time index $k_{\mathrm{G}}+s$ can be written as

$$\tilde{\mathbf{J}}^{2}_{\xi_{k_{\mathrm{G}}+s}} = \sum_{j\in \mathbf{i}_{k_{\mathrm{G}}+s}} \left[P_{j,l}\bar{\mathbf{H}}^{T}_{j,k_{\mathrm{G}}+s}\mathbf{Y}^{-1}_{j,k_{\mathrm{G}}+s}\bar{\mathbf{H}}_{j,k_{\mathrm{G}}+s} \right] \tag{44}$$

Mathematically speaking, the target motion information matrix $\mathbf{J}^{1}_{\xi_{k_{\mathrm{G}}+s}}$ at time index $k_{\mathrm{G}}+s$ needs to be calculated as (43) by integrating both $\mathbf{J}^{1}_{\xi_{k_{\mathrm{G}}+s-1}}$ and $\mathbf{J}^{2}_{\xi_{k_{\mathrm{G}}+s-1}}$ at the iteration step. Instead of that, the relaxed target motion information is defined as

$$\begin{aligned}\tilde{\mathbf{J}}^{1}_{\xi_{k_{\mathrm{G}}+s}} =& \Big[\mathbf{Q}_{\xi}\left(k_{\mathrm{G}}+s,k_{\mathrm{G}}+s-1\right)+ \\ & \mathbf{F}\left(k_{\mathrm{G}}+s,k_{\mathrm{G}}+s-1\right)\left(\tilde{\mathbf{J}}^{1}_{\xi_{k_{\mathrm{G}}+s-1}}\right)^{-1}\mathbf{F}^{T}\left(k_{\mathrm{G}}+s,k_{\mathrm{G}}+s-1\right)\Big]^{-1}\end{aligned} \tag{45}$$

With some mathematical derivation, it easy for us to know that

$$\begin{aligned}\tilde{\mathbf{J}}^{1}_{\xi_{k_{\mathrm{G}}+s}} &= \left[\mathbf{Q}_{\xi}\left(k_{\mathrm{G}}+s,k_{\mathrm{G}}+s-1\right)+\mathbf{F}\left(k_{\mathrm{G}}+s,k_{\mathrm{G}}+s-1\right)\left(\tilde{\mathbf{J}}^{1}_{\xi_{k_{\mathrm{G}}+s-1}}\right)^{-1}\mathbf{F}^{T}\left(k_{\mathrm{G}}+s,k_{\mathrm{G}}+s-1\right)\right]^{-1} \\ &\ \ \vdots \\ &= \left[\mathbf{Q}_{\xi}\left(k_{\mathrm{G}}+s,k_{\mathrm{G}}\right)+\mathbf{F}\left(k_{\mathrm{G}}+s,k_{\mathrm{G}}\right)\left(\tilde{\mathbf{J}}^{1}_{\xi_{k_{\mathrm{G}}}}\right)^{-1}\mathbf{F}^{T}\left(k_{\mathrm{G}}+s,k_{\mathrm{G}}\right)\right]^{-1} \\ &= \left[\mathbf{Q}_{\xi}\left(k_{\mathrm{G}}+s,k_{\mathrm{AP},l}\right)+\mathbf{F}\left(k_{\mathrm{G}}+s,k_{\mathrm{AP},l}\right)\mathbf{J}^{-1}\left(\xi_{k_{\mathrm{AP},l}}\right)\mathbf{F}^{T}\left(k_{\mathrm{G}}+s,k_{\mathrm{AP},l}\right)\right]^{-1}\end{aligned} \tag{46}$$

Hence, by summarizing the above defined target motion information at time index $k_{\mathrm{AP},l+1}$ and all the measurement information during the l th allocation period, the *relaxed BIM* (R-BIM) can be obtained as

$$\begin{aligned}\mathbf{J}^{\text{R-CRLB}}_{\xi_{k_{\mathrm{AP},l+1}}}\left(\mathbf{p}_{l}\right) &= \tilde{\mathbf{J}}^{1}_{\xi_{k_{\mathrm{AP},l+1}}}+\sum_{s=0}^{M_{l,k_{\mathrm{G}}}}\tilde{\mathbf{J}}^{2}_{\xi_{k_{\mathrm{G}}+s}} \\ &= \Big[\mathbf{Q}_{\xi}\left(k_{\mathrm{AP},l+1},k_{\mathrm{AP},l}\right)+\mathbf{F}\left(k_{\mathrm{AP},l+1},k_{\mathrm{AP},l}\right)\mathbf{J}^{-1}\left(\xi_{k_{\mathrm{AP},l}}\right)\mathbf{F}^{T}\left(k_{\mathrm{AP},l+1},k_{\mathrm{AP},l}\right)\Big]^{-1} \\ &\quad +\sum_{s=0}^{M_{l,k_{\mathrm{G}}}}\sum_{j\in\mathbf{i}_{k_{\mathrm{G}}+s}}\left[P_{j,l}\bar{\mathbf{H}}^{T}_{j,k_{\mathrm{G}}+s}\mathbf{Y}^{-1}_{j,k_{\mathrm{G}}+s}\bar{\mathbf{H}}_{j,k_{\mathrm{G}}+s}\right]\end{aligned} \tag{47}$$

Intuitively speaking, the R-BIM is the same as the BIM calculated for a synchronized scenario [7], in which all the measurements from different radar during the l th allocation period are assumed to be obtained at time index $k_{\mathrm{AP},l+1}$.

APPENDIX B

Prove that $\mathbb{S}\left(\mathbf{p}_{l}\right)$ is convex

The objective function $\mathbb{S}\left(\mathbf{p}_{l}\right)$ defined in (36) is of the following form

$$\mathbb{S}\left(\mathbf{p}_{l}\right)=\sqrt{\mathrm{Tr}_{n_{\mathbf{x}}}\left(\mathbf{\Lambda}\mathbf{C}^{\text{R-CRLB}}_{\xi_{k_{\mathrm{AP},l+1}}}\left(\mathbf{p}_{l}\right)\mathbf{\Lambda}^{T}\right)} \tag{48}$$

where $\mathbf{C}^{\text{R-CRLB}}_{\xi_{k_{\mathrm{AP},l+1}}}\left(\mathbf{p}_{l}\right)=\left[\mathbf{J}^{\text{R-CRLB}}_{\xi_{k_{\mathrm{AP},l+1}}}\left(\mathbf{p}_{l}\right)\right]^{-1}$. To facilitate derivation, we set

$$\begin{cases}\mathbf{U}_{l+1}=\left[\mathbf{Q}_{\xi}\left(k_{\mathrm{AP},l+1},k_{\mathrm{AP},l}\right)+\mathbf{F}\left(k_{\mathrm{AP},l+1},k_{\mathrm{AP},l}\right)\mathbf{J}^{-1}_{\xi_{k_{\mathrm{AP},l}}}\left(\mathbf{p}_{l}\right)\mathbf{F}^{T}\left(k_{\mathrm{AP},l+1},k_{\mathrm{AP},l}\right)\right]^{-1}, \\ \mathbf{V}_{j,k_{\mathrm{G}}+s}=\left[\bar{\mathbf{H}}^{T}_{j,k_{\mathrm{G}}+s}\mathbf{Y}^{-1}_{j,k_{\mathrm{G}}+s}\bar{\mathbf{H}}_{j,k_{\mathrm{G}}+s}\right]\end{cases} \tag{49}$$

and thus the R-BIM in (47) can be reformulated as

$$\mathbf{J}^{\text{R-CRLB}}_{\xi_{k_{\mathrm{AP},l+1}}}\left(\mathbf{p}_{l}\right)=\mathbf{U}_{l+1}+\sum_{s=0}^{M_{l,k_{\mathrm{G}}}}\sum_{j\in\mathbf{i}_{k_{\mathrm{G}}+s}}P_{j,l}\mathbf{V}_{j,k_{\mathrm{G}}+s} \tag{50}$$

According to (14) and (17), we know that matrix $\mathbf{Y}_{j,k_{\mathrm{G}}+s}$ is a $n_{\mathbf{z}}\times n_{\mathbf{z}}$ diagonal matrix. Thus, it is easy for us to prove that $\mathbf{U}_{l+1}$ and $\mathbf{V}_{j,k_{\mathrm{G}}+s}$ are two symmetric positive definite matrices, if the initial BIM $\mathbf{J}\left(\xi_{k_{\mathrm{AP},0}}\right)\in S^{n_{\mathbf{x}}+2N}_{++}$, where $S^{n_{\mathbf{x}}+2N}_{++}$ denotes the set of symmetric positive definite matrices with a dimension of $\left(n_{\mathbf{x}}+2N\right)\times\left(n_{\mathbf{x}}+2N\right)$.

According to (48), we see that (50) is actually a composition of a function $\mathrm{Tr}_{n_{\mathbf{z}}}\left(\mathbf{\Lambda}\mathbf{X}^{-1}\mathbf{\Lambda}^{T}\right)$ and an affine transformation $\mathbf{X}\to\mathbf{U}_{l+1}+\sum_{s=0}^{M_{l,k_{\mathrm{G}}}}\sum_{j\in\mathbf{i}_{k_{\mathrm{G}}+s}}P_{j,l}\mathbf{V}_{j,k_{\mathrm{G}}+s}$. In this scenario, one can say that $\mathbb{S}\left(\mathbf{p}_{l}\right)$ is convex on [31] the set

$$\left\{\mathbf{p}_{l}\left|\left[\mathbf{U}_{l+1}+\sum_{s=0}^{M_{l,k_{\mathrm{G}}}}\sum_{j\in\mathbf{i}_{k_{\mathrm{G}}+s}}P_{j,l}\mathbf{V}_{j,k_{\mathrm{G}}+s}\right]\in S^{n_{\mathbf{x}}+2N}_{++}\right.\right\}, \tag{51}$$

if one can prove that $\mathrm{Tr}_{n_{\mathbf{z}}}\left(\mathbf{\Lambda}\mathbf{X}^{-1}\mathbf{\Lambda}^{T}\right)$ is convex on $\mathbf{X}\in S^{n_{\mathbf{x}}+2N}_{++}$.

For the function $f\left(\mathbf{X}\right)=\mathrm{Tr}_{n_{\mathbf{z}}}\left(\mathbf{\Lambda}\mathbf{X}^{-1}\mathbf{\Lambda}^{T}\right)$, we can verify its concavity by considering an arbitrary line, given by $\mathbf{X}=\mathbf{Z}+t\mathbf{V}$, where $\mathbf{Z},\mathbf{V}\in S^{n_{\mathbf{x}}+2N}$. We define $g\left(t\right)=f\left(\mathbf{Z}+t\mathbf{V}\right)$, and restrict g to the interval of values of t for which $\mathbf{Z}+t\mathbf{V}>0$. With loss of generality, we can assume that $t=0$ is inside this interval, i.e. $\mathbf{Z}>0$. An intuitive explanation for this assumption is that, $\mathbf{Z}$, which represents the BIM of the prior information, is indeed a symmetric positive definite matrix. Then, we have

$$\begin{aligned}g\left(t\right) &= \mathrm{Tr}_{n_{\mathbf{z}}}\left[\mathbf{\Lambda}\left(\mathbf{Z}+t\mathbf{V}\right)^{-1}\mathbf{\Lambda}^{T}\right] \\ &= \mathrm{Tr}_{n_{\mathbf{z}}}\left[\mathbf{\Lambda}\mathbf{Z}^{-1/2}\left(\mathbf{I}+t\mathbf{Z}^{-1/2}\mathbf{V}\mathbf{Z}^{-1/2}\right)^{-1}\mathbf{Z}^{-1/2}\mathbf{\Lambda}^{T}\right] \\ &= \mathrm{Tr}_{n_{\mathbf{z}}}\left[\mathbf{\Lambda}\mathbf{Z}^{-1/2}\mathbf{Q}\left(\mathbf{I}+t\mathbf{\Pi}\right)^{-1}\mathbf{Q}^{T}\mathbf{Z}^{-1/2}\mathbf{\Lambda}^{T}\right] \\ &= \mathrm{Tr}_{n_{\mathbf{z}}}\left[\mathbf{Q}^{T}\mathbf{Z}^{-1/2}\mathbf{\Lambda}^{T}\mathbf{\Lambda}\mathbf{Z}^{-1/2}\mathbf{Q}\left(\mathbf{I}+t\mathbf{\Pi}\right)^{-1}\right] \\ &= \sum_{i=1}^{n_{\mathbf{z}}}\left(\mathbf{Q}^{T}\mathbf{Z}^{-1/2}\mathbf{\Lambda}^{T}\mathbf{\Lambda}\mathbf{Z}^{-1/2}\mathbf{Q}\right)_{ii}\left(1+t\pi_{i}\right)^{-1}\end{aligned} \tag{52}$$

where we used the eigenvalue decomposition $\mathbf{Z}^{-1/2}\mathbf{V}\mathbf{Z}^{-1/2}=\mathbf{Q}\mathbf{\Pi}\mathbf{Q}^{T}$. In the last equality, we express $g\left(t\right)$ as a positive weighted sum of convex function $\left(1+t\pi_{i}\right)^{-1}$, and thus we can conclude that $f\left(\mathbf{X}\right)=\mathrm{Tr}_{n_{\mathbf{z}}}\left(\mathbf{\Lambda}\mathbf{X}^{-1}\mathbf{\Lambda}^{T}\right)$ is convex.

REFERENCES

[1] R. Nadjiasngar, A. Charlish, "A performance model for target tracking with a radar network, " *in Proceedings of IEEE Radar Conference*, Johannesburg, South Africa, 2015, pp. 238-243

[2] C.J. Baker, and A.L, Hume, "Netted radar sensing, " *IEEE Aerospace and Electronic Systems Magazine*, vol. 18, no. 2, pp. 3–6, Feb. 2003.

[3] V. Chernyak, "Multisite radar systems composed of MIMO radars, " *IEEE Aerospace and Electronic Systems Magazine*, vol. 29, no. 12, pp. 28–37, Dec. 2014

[4] J. K. Yan, H. W. Liu, and B. Jiu, et al., "Simultaneous multibeam resource allocation scheme for multiple target tracking, " *IEEE Transactions on Signal Processing*, vol. 63, no. 12, pp. 3110–3122, Jun. 2015.

[5] N. H. Nguyen, K. Doğançay, L. M. Davis, "Adaptive waveform and Cartesian estimate selection for multistatic target tracking, " *Signal Processing*, vol. 111, pp. 13-25, Nov. 2015.

[6] J. K. Yan, H. W. Liu, and B. Jiu, et al., "Joint detection and tracking processing algorithm for target tracking in multiple radar system," *IEEE Sensors Journal*, vol. 15, no. 11, pp. 6534-6541, Nov. 2015.

[7] J. K. Yan, H. W. Liu, and B. Jiu, et al., "Power allocation algorithm for target tracking in unmodulated continuous wave radar network, " *IEEE Sensors Journal*, vol. 15, no. 2, pp. 1098–1108, Feb. 2015.

[8] N. Sharaga, J. Tabrikian, H. Messer, "Optimal cognitive beamforming for target tracking in MIMO radar/sonar, " *IEEE Journal of Selected Topics in Signal Processing*, vol. 9, no. 8, pp. 1440-1450, Dec. 2015.

[9] R. A. Romero, N. A. Goodman. "Cognitive radar network: cooperative adaptive beamsteering for integrated search-and-track application, " *IEEE Transactions on Aerospace and Electronic Systems*, vol. 49, no. 2, pp. 915–931, Apr. 2013.

[10] A. Aubry, A. De Maio, and B. Jiang, et al, "Ambiguity function shaping for cognitive radar via complex quartic optimization," *IEEE Transactions on Signal Processing*, vol. 61, no. 22, pp. 5603-5619, Jul. 2013.

[11] P. Willett, R. Niu, and Y. Bar-Shalom, "Integration of Bayes detection with target tracking, " *IEEE Transactions on Signal Processing*, vol. 49, no. 1, pp. 17–29 , Jan. 2001.

[12] M. Fatemi, S. Haykin, "Cognitive control: Theory and application, " *IEEE Access*, vol. 2, pp. 698-710. Jun. 2014.

[13] H. W. Liu, S. H. Zhou, H. L. Liu, et al., "Radar detection during tracking with constant track false alarm rate," in *Proceedings of IEEE International Radar Conference*, Lille, France, 2014, pp. 1-5.

[14] M. S. Aslan, A. Saranlı, "*Joint Optimization of Detection and Tracking in Adaptive Radar Systems*," Berlin Heidelberg: Springer, 2013.

[15] W. Zhao and G. Li, "On the detection probability of sparse signals with sensor networks based on distributed subspace pursuit," in *Proceedings of The Third IEEE China Summit and International Conference on Signal and Information Processing*, Chengdu, China, 2015, pp. 324-328.

[16] G. Li, T. Wimalajeewa, and P. K. Varshney,"Decentralized and collaborative subspace pursuit: A communication-efficient algorithm for joint sparsity pattern recovery with sensor networks," *IEEE Transactions on Signal Processing*, vol. 64, no. 3, pp. 556-566, Feb. 2016.

[17] P. Chavali, A. Nehorai, "Scheduling and Power Allocation in a Cognitive Radar Network for Multiple-Target Tracking, " *IEEE Transactions on Signal Processing*, vol. 60, no. 2, pp. 715-729, Feb. 2012.

[18] A. Turlapaty, Y. Jin, "Bayesian sequential parameter estimation by cognitive radar with multiantenna arrays, " *IEEE Transactions on Signal Processing*, vol. 63, no. 4, pp. 974-987, Feb. 2015.

[19] B. Ristic, S. Arulampalam, and N. Gordon, "*Beyond the Kalman Filter: Particle Filters for Tracking Applications*, " Norwell, MA: Artech House, 2004.

[20] N. Levanon, *Radar Principles,* 1st ed New York, NY: John Wiley and Sons, 1988.

[21] S. Blackman, R. Dempster, T. Broida, "Multiple hypothesis track confirmation for infrared surveillance systems, " *IEEE Transactions on Aerospace and Electronic Systems,* vol. 29, no. 3, pp. 810-824, Jul. 1993.

[22] E. Birgin, J. Martinez, and M. Raydan, "Nonmonotone spectral projected gradient methods on convex sets," *SIAM Journal on Optimization*, vol. 10, no. 4, pp. 1196–1211, Jun. 2000.

[23] A. T. Alouani, J. E. Gray, D. H. McCabe, "Theory of distributed estimation using multiple asynchronous sensors, " *IEEE Transactions on Aerospace and Electronic Systems*, vol. 41, no. 2, pp. 717-722, Apr. 2005.

[24] Y. Bar-Shalom, X. R. Li, and T. Kirubarajan. "*Estimation with Applications to Tracking and Navigation,* " New York, NY: John Wiley and Sons, 2001: 199-295.

[25] V. A. Bavdekar, A. P. Deshpande, S. C. Patwardhan, "Identification of process and measurement noise covariance for state and parameter estimation using extended Kalman filter, " *Journal of Process control*, Vol. 21, No. 4, pp. 585-601, Apr. 2011.

[26] H. L. Van Trees, "*Optimum Array Processing: Detection, Estimation, and Modulation Theory, Part IV*, " New York, NY: John Wiley and Sons, 2002.

[27] M. E. Liggins, D. L. Hall, and J. Llinas, Eds., "*Handbook of Multisensor Data Fusion: Theory and Practice,*" Boca Raton, FL: CRC, 2nd ed. 2009.

[28] J. K. Yan, B. Jiu, and H. W. Liu, et al., "Prior knowledge based simultaneous multibeam power allocation algorithm for cognitive multiple targets tracking in clutter, " *IEEE Transactions on Signal Processing*, vol. 63, no. 2, pp. 512–527, Jan. 2015.

[29] X. Song, P. Willett, S. Zhou, "On Fisher information reduction for range-only localization with imperfect detection, " *IEEE Transactions on Aerospace and Electronic Systems*, Vol. 48, No. 4, pp. 3694–3702, Oct. 2012.

[30] V. D. Blondel, S. Boyd, and H. Kimura, *Recent Advances in Learning and Control*. New York: Springer, 2008.

[31] S. Boyd and L. Vandenberghe, "*Convex Optimization*," Cambridge, U.K.: Cambridge Univ. Press, 2004.

AUTHOR PHOTOS AND BIOGRAPHIES

Junkun Yan (M'16) was born in Sichuan, China, 1987. He received the B.S. and Ph.D. degrees in electronics engineering from Xidian University, Xi'an, China, in 2009 and 2015, respectively. He is now a researcher with the National Laboratory of Radar Signal Processing, Xidian University. His research interests include adaptive signal processing, target tracking, and cognitive radar.

Hongwei Liu(M'00) received the M.S. and Ph.D. degrees, both in Electronic Engineering, from Xidian University, Xi'an, China, in 1995 and 1999, respectively. He worked at the National Laboratory of Radar Signal Processing, Xidian University, after that. From 2001 to 2002, he was a visiting scholar at the Department of Electrical and Computer Engineering, Duke University, Durham, NC.

He is currently a Professor at the National Laboratory of Radar Signal Processing, Xidian University. His research interests are radar automatic target recognition, radar signal processing, and adaptive signal processing.

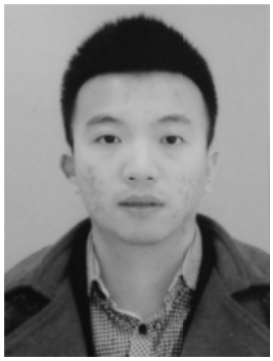

Wenqiang Pu was born in Sichuan, China, 1991. He received the B.S. degree in electronics engineering from Xidian

University, Xi'an, China, in 2013. He is currently pursuing the Ph.D. degree with the National Laboratory of Radar Signal Processing, Xidian University. His research interests include collaborative signal processing, and target tracking.

Hongliang Liu was born in Hebei, China, 1989. He received the B.S. degree in applied physics from Xidian University, Xi'an, China, in 2011. He is currently pursuing the Ph.D. degree with the National Laboratory of Radar Signal Processing, Xidian University. His research interests include target detection, target tracking, and collaborative signal processing.

Zheng Bao (M'80-SM'90-LSM'04) was born in Jiangsu, China. Currently, he is a professor with Xidian University and the chairman of the academic board of the National Key Lab of Radar signal Processing. He has authored or co-authored 6 books and published over 300 papers. Now, his research fields include space-time adaptive processing (STAP), radar imaging (SAR/ISAR), automatic target recognition (ATR) and over-the-horizon radar (OTHR) signal processing.
Professor Bao is a member of the Chinese Academy of Sciences.